Design and Performance Evaluation of Vertical Shafts

Part I: Rational Shaft Design Method
Part II: Verification of Design Method

by

R.C.K. Wong* and P.K. Kaiser**

*ESSO Resources Canada Ltd.
Calgary, Alberta
**Professor of Civil Engineering
Department of Civil Engineering
University of Alberta
Edmonton, Canada, T6G 2G7
(403) 432-5106

# ABSTRACT

Ground deformations around axisymmetric shafts cannot be determined with the currently available design approaches which are mostly based on plasticity methods. The Convergence/Confinement Method (usually applied to tunnels) with consideration of gravitational effects and the three-dimensional conditions near a shaft, is proposed as a tool to predict the formation pressure on a shaft and the radial ground displacements. It is shown that the behaviour of a shaft is governed by: (1) the mode of yield initiation dominated by the in-situ stress state and the soil strength parameters, and (2) the extent of the yield zone that develops if wall displacements are allowed to occur during construction.

Closed-form solutions are presented to approximate the pressure/displacement relationship for cohesionless and cohesive soils. Results from this approach compare well with those obtained by finite element analyses. The conventional methods provide minimum support pressures that are required to maintain stability but are generally less than those actually encountered if ground movements are restricted during construction with good ground control.

## 1. INTRODUCTION

The design of a shaft in soil consists of two main steps: (1) design of the shaft lining to prevent instability of shaft wall, and (2) estimation of the soil movement associated with shaft construction. Although these two tasks are interrelated, they are usually handled separately. Except for simplicity, there are no practical reasons why one should separate the determination of lining pressure and ground deformation.

Most of the currently available design approaches are based on soil plasticity considerations or plasticity equilibrium methods (PEM), e.g., Terzaghi (1943) and Berezantzev (1958), whereby the formation pressures on the shaft lining are determined by satisfying equilibrium of yielded, plastic ground behind the support. Alternatively, limit equilibrium methods (LEM), assuming hypothetical rupture surfaces are used for design, e.g. Prater (1977). The actually expected and observed pressures depend, however, on such factors as ground deformation, in-situ stress, and ground strength/deformation properties. They differ substantially from those predicted by the methods mentioned above. Most importantly, the actual pressures are often greater than those predicted in this manner.

No closed-form solutions are currently available for the determination of shaft wall displacements and movements of the surrounding ground. In practice, the displacements are often controlled or limited by choice of a suitable factor of safety and excessive yielding is prevented by an appropriate construction sequence.

The Convergence/Confinement Method (CCM), which accounts for most relevant design parameters (e.g., in-situ stress field, ground and support properties, and construction sequence), provides an analytical framework to predict the formation pressure and the soil deformation simultaneously. So far, it has

only been applied successfully to circular, horizontal underground openings where the stress component parallel to the axis of the opening has little effect on the opening behaviour and where the three-dimensional conditions near the tunnel face can be approximated.

Since the analysis of a shaft near the ground surface is a truly three-dimensional problem, the CCM in its common form is not adequate to describe the behaviour of a shaft. The effect of gravity or vertical forces must be considered. This can be achieved by combination of plasticity or limit equilibrium techniques with the CCM. In this manner, the ground convergence curve for the shaft wall can be derived and the required support pressure can be rationally assessed. The limits of applicability of conventional methods for shaft design can then be evaluated properly and field measurements can be interpreted based on a rational shaft performance model.

The scope of this paper is to establish typical shaft behavioural modes and to quantify the responses of a shaft to excavation, by use of the convergence/confinement concept, in terms of support pressure and radial wall displacement. First, conventional design methods are briefly and critically reviewed, and the proposed Convergence/Confinement Method is introduced. Behavioural modes ranging from elastic response, through yield initiation and propagation to ultimate collapse, are discussed. In the second part, results of the proposed CCM and the conventional design methods are compared with results from finite element analyses. Throughout the paper it is assumed that the magnitude of the horizontal stresses is independent of its orientation ($\sigma_h = \sigma_H$).

The technique proposed in this paper has also been applied to several case histories reported by Lade et al. (1981), Müller-Kirchenbauer et al. (1980), and Wong and Kaiser (1984), and good agreement was observed. The results of this comparison will be presented in a later publication.

# 2. REVIEW OF PREVIOUSLY PROPOSED SHAFT DESIGN TECHNIQUES

Two groups of basic shaft design models can be identified: those considering gravity or the influence of the vertical principal stress (e.g., Terzaghi (1943); Berezantzev (1958); Prater (1977)) and those treating a shaft as a two-dimensional, 'hole-in-a-plate' problem (e.g., Abel et al., 1979). As will be seen, the latter approach is only valid under certain field stress conditions.

In all cases, support pressures are calculated that correspond to one specific, often limiting, state of equilibrium and various design criteria are evoked to ensure acceptable performance in terms of ground deformation. A factor of safety is applied to gain a sufficiently large margin against failure or to control deformations. Alternatively, stability and serviceability are achieved by provision of sufficient support pressure to avoid onset of plasticity (allowable stress design). These approximate methods of controlling deformations provide safety margins of unknown magnitude. Some conservative designers still support the concept of design for the virgin state of stress and are willing to accept high support cost to ensure an unnecessarily high and unknown safety margin.

These design approaches are not intended to predict the actual conditions in the field. They provide either a lower limit of support pressure that is needed to prevent collapse or a design pressure that should never be exceeded in reality. For comparison with field measurements, a performance model, such as the one presented later, is required that predicts the actual conditions for a given construction sequence. Most of the conventional methods are design and not performance models.

## 2.1 Terzaghi's Method

Terzaghi (1943) already recognized that the problem of shaft design was not as simple as merely rotating a tunnel in a weightless medium and provided an elegant, approximate solution

for considering the effect of gravity, if it dominates shaft behaviour. He assumed that stress concentrations near a vertical hole would cause yielding due to the stress difference between tangential and radial stresses in an annulus around a shaft (Mode A: due to $(\sigma_t - \sigma_r)$; see Fig.1.a)). Even though the tangential stresses are generally greater than the vertical, equalization of vertical and tangential stresses near the shaft was assumed. Based on this approximate stress distribution, the limit equilibrium state of a downward sliding, cylindrical element of yielded ground was assessed. Hence, the support pressure calculated by Terzaghi (1943) is the minimum pressure required to prevent this mode of instability.

An example of this critical support pressure distribution is shown for a cohesionless soil in Fig.2. It is only valid if vertical plasticity and Mode A-type yielding is possible, i.e., at high $K_0$-values as will be demonstrated later.

Terzaghi noticed that his solution neglected the effect of principal stress rotation near the shaft due to non-zero shear stresses (McCreath, 1980) and proposed the use of a reduced friction angle $\phi*$:

$$\phi* = (\phi-5°) \text{ for } 30° < \phi < 40° \text{ and } c = 0$$

for the Mohr-Coulomb failure criterion.

## 2.2 Berezantzev's Method

Berezantzev (1958) proposed a method of earth pressure calculation for cylindrical retaining walls whereby the state of stress around the shaft is described by two differential equations of equilibrium. He used the Mohr-Coulomb failure criterion as a condition of plastic equilibrium and also made the assumption of equal principal stresses $(\sigma_t = \sigma_v = \sigma_1, \sigma_r = \sigma_3)$ to render the problem statically determinate. However, only one set of slip surfaces (Mode B: due to $(\sigma_v - \sigma_r)$) is assumed to occur inside the yielded soil (Fig.1.b).

The earth pressure is determined by Sokolovsky's numerical 'step-by-step' computation technique. An example of the resulting earth pressure distribution is shown in Fig.2. It is almost identical to the one predicted by Terzaghi. However, Berezantzev's approach predicts sliding along a set of nearly cone-shaped surfaces. With the assumption of equal major principal stresses, Mode A-type yielding along a set of vertical planes is also possible to facilitate sliding along the conical surfaces.

## 2.3 Prater's Method

Prater (1977) approximated the sliding surface predicted by Berezantzev by a cone and conducted a limit equilibrium analysis assuming a Mohr-Coulomb failure criterion for the sliding surface. At the vertical sides of a pie-shaped element, he introduced a wedging force T with a radial outward component and argued that a coefficient $\lambda$ for the determination of T should fall between the active earth pressure coefficient $K_a$ and the coefficient at rest $K_0$ and that it should not be unity as assumed by Terzaghi or Berezantzev. The resulting earth pressure distribution, shown in Fig.2 for a cohesionless soil, indicates that this analysis leads to the unreasonable result of zero support pressure requirement for stability of a deep shaft (e.g., $H/a > 9$ for $\phi = 30°$, $c = 0$).

This deficiency must be attributed to the fact that the magnitude of the wedging force T is not limited. At depth, this force is actually controlled by Mode A-type failure stresses and cannot, as implicit in Prater's analysis, reach infinity at great depth. Prater's approach does not predict a critical (minimum) support pressure, as Terzaghi, but the earth pressure at the *initiation* of Mode B-type failure. Lower radial support pressures are sufficient to maintain stability if stress redistribution due to Mode A-type yielding is permitted during shaft wall deformation. This is illustrated by Fig.1.b. For $K_0$ less than a critical value $K_{cr}$ (to be defined later), radial stresses may

decrease while tangential stresses increase until failure occurs due to the deviatoric stress difference $(\sigma_v - \sigma_r)$ in Mode B. At this point, $\lambda = (\sigma_t/\sigma_{vo})$ is somewhat greater than $K_0$ and the earth pressure can be reasonably well predicted by Prater's method ($\lambda = K_0$). However, a further reduction of the radial pressure will cause arching as illustrated by Fig.3 and the vertical stress will drop while the tangential stress increases. Ultimately, vertical and tangential stresses equalize when the ground yields in both modes, A and B. This ultimate condition is modelled by Berezantzev and approximated by Terzaghi. Prater's method does not predict the same minimum pressure required to maintain stability. It is too conservative at shallow depth and too unconservative at greater depth.

## 2.4 'Hole-in-a-Plate' Approach

Many authors have developed analytical procedures to calculate the extent of yielding, the equilibrium support pressure and the related deformations for circular openings in a uniform stress field and in perfectly plastic or strain-weakening ground (e.g., Brown et al., 1983). These methods provide the ground convergence curve which can be combined with the support confinement curve to predict an equilibrium state of ground/support interaction. Mode A-type failure is tacitly assumed for this approach.

An early attempt to apply this concept for the interpretation of field measurements was presented by Abel et al. (1979) in a back analysis of a well documented deep shaft. In their calculation of lining pressures, they neglected the rock displacements before liner installation but considered the effect of elastic, shrinkage and creep deformations of the liner. In a re-evaluation of this case history, McCreath (1980) found that the CCM could be applied successfully to explain without consideration of gravity the shaft performance of this deep shaft in yielding rock. Because ground deformations were restricted by the shaft support, the measured ground pressures exceeded, as

would be expected, the minimum pressures predicted by the methods proposed by Terzaghi and Berezantzev.

In summary, the existing methods are tied to specific conditions and thus none of them permits to predict the actual shaft performance. These methods do not indicate when gravity effects are relevant or when the limits of applicability of the 'hole-in-a-plate' approach have been reached. These deficiencies are largely overcome by the proposed design method described in the following.

## PART I - NEW SHAFT DESIGN METHOD

## 3. PROPOSED SHAFT DESIGN AND PERFORMANCE PREDICTION METHOD

The Convergence/Confinement Method (CCM) provides a conceptual framework that can be analytically formulated to predict the interrelationship between stresses and displacements in the soil near an underground opening (e.g., Fenner, 1939; and Pacher, 1964). The extent of the yield (or plastic) zone can also be estimated by this method under certain, well-defined conditions. The CCM is adopted and proposed in the following as a rational approach to predict shaft behaviour. In this manner most relevant factors (e.g., in situ stress, soil strength and deformation properties as well as many construction details) can be included in the analysis.

The behaviour of a shaft is affected and near the surface dominated by gravitational forces. It is a truly three-dimensional problem and all three stress components ($\sigma_t$, $\sigma_v$ and $\sigma_r$) must be considered. The mode of yielding, its initiation and propagation, depends on the relative magnitude of these stresses and, hence, on the initial in-situ state of stress or $K_0$. In order to apply the two-dimensional 'hole-in-a-plate' model to determine the relationship between support pressure and shaft wall displacement, it is necessary to understand the mechanisms of shaft behaviour so that an adjustment can be made to the CCM.

The excavation of a shaft can be simulated by a stress relief ($\Delta\sigma_r$ at the shaft wall) causing the surrounding soil to deform both horizontally and vertically. Excessive stress relief will induce yielding near the opening causing permanent plastic deformations. The magnitude of support pressure, wall displacement and extent of plastic zone are related. The stress relief during shaft excavation causes stress redistribution near the opening, and thus induces vertical and horizontal arching as illustrated by Fig.3. Furthermore, a horizontal hoop stress increase is induced in a horizontal plane, i.e., in the tangential direction. Vertical arching with convex downward stress trajectories (Handy, 1985) arises when a plastic zone of limited extent tends to move vertically downward. It develops one-sided or between the shaft support and the surrounding unyielded soil mass. Collapse is prevented if stable arches can be maintained by sufficient support pressure.

In the following, the relationship between the support pressure, $p_i$, the extent of the plastic zone, R, and the wall displacement, $u_i$, or the ground convergence curve (GCC) is derived considering horizontal and vertical arching.

It must be stressed that the proposed model is a performance prediction and not a design model. Adequate safety margins must be introduced by application of reasonable design criteria to ensure satisfactory shaft performance.

## 3.1 Horizontal Arching

### 3.1.1 Support Pressure

Prior to excavation, a soil element adjacent to the shaft wall is subjected to in-situ stresses. The excavation of the shaft may be simulated by progressively reducing the support pressure (or radial stress). For the axisymmetric case in elastic soil, the stress distributions are given by Eqns.1 to 3 (Terzaghi, 1943). For notations see Appendix A.

$$\sigma_{vo} = \gamma h = p_o \qquad (1)$$

$$\sigma_r = K_o p_o - [K_o p_o - p_i](a/r)^2 \qquad (2)$$

$$\sigma_t = K_o p_o + [K_o p_o - p_i](a/r)^2. \qquad (3)$$

These equations are derived based on the following assumptions: (i) $\sigma_v$, $\sigma_r$ and $\sigma_t$ are principal stresses, (ii) shear stresses along the shaft wall are negligible, and (iii) the bottom of the shaft is remote.

As $p_i$ is reduced, the stress differences increase and the strength of the soil may be exceeded. The onset of the plasticity and the mode of yield initiation depends on the value of $K_o$ and the strength parameters of the soil. For simplicity, the following derivations are for cohesionless materials only. The formulations for cohesive soils are given in Appendix B.

For a purely frictional, elastic, perfectly plastic material with a linear Mohr-Coulomb failure criterion, the maximum stress ratio which may be sustained is:

$$\sigma_1/\sigma_3 = N = \tan^2(\pi/4 + \phi/2). \qquad (4)$$

Three modes of yield initiation can be calculated from Eqns.1 to 3, and the corresponding support pressures, $p_i$, are:

A) For $(\sigma_t - \sigma_r)$: $p_i = 2K_o p_o/(N+1)$ $\qquad (5)$

B) For $(\sigma_v - \sigma_r)$: $p_i = p_o/N$ $\qquad (6)$

C) For $(\sigma_t - \sigma_v)$: $p_i = (2K_o - N)p_o.$ $\qquad (7)$

The largest value of $p_i$ will govern which mode of yield initiation occurs. In terms of $K_o$-values, failure is initiated if for:

Mode A: $(N+1)/2N < K_o < (N+1)/2$ $\qquad (8)$

$$\text{Mode B: } K_o < (N+1)/2N \qquad \qquad (9)$$

$$\text{Mode C: } K_o > (N+1)/2 \ . \qquad \qquad (10)$$

For cohesionless soil with $\phi = 30°$ or $N = 3$ in:

Mode A for: $0.67 < K_o < 2.0$ (Fig.1.a);

Mode B for: $K_o < 0.67$ (Fig.1.b); and

Mode C for: $K_o > 2.0$ (Fig.1.c).

Mode A is the mode commonly evaluated for tunnels in yielding ground. Mode C, although possible, has been neglected in the following analysis because it is seldom of practical significance in soft ground.

The boundary between the two remaining modes of yield initiation is then given by a critical $K_o$-value: $K_{cr} = (N+1)/2N$. For each of these two modes, the relationship of support pressure and extent of plastic zone can be derived separately.

3.1.1.a) **Initiation of Yielding of Mode A at $K_o > K_{cr}$ (Fig.4.a):**

Fig.4.b shows the sequential stages of stress distribution for Mode A as the internal support pressure is reduced.

During the first stage (Fig.4.b.(1)), the vertical stress remains constant, the radial stress decreases while the tangential stress increases according to Eqns.1 to 3. Yield initiation of Mode A occurs if the condition:

$$\sigma_t/\sigma_r = N \text{ or } p_i = 2K_o p_o/(N+1) \qquad \qquad (11)$$

is reached. The vertical stress at yield initiation always acts as an intermediate stress.

Further reduction of the fictitious internal support pressure causes the propagation of a plastic zone, and the tangential stress decreases to satisfy the failure criteria

(Fig.4.b.(2)). The extent of the plastic zone is (Ladanyi, 1974):

$$R_{tr} = a[2K_o p_o/(N+1)p_i]^{1/(N-1)} \tag{12}$$

and the stresses within the plastic zone $(r < R_{tr})$ are:

$$\sigma_r = p_i \, (r/a)^{N-1} \tag{13}$$

$$\sigma_t = Np_i \, (r/a)^{N-1} \ . \tag{14}$$

As the tangential stress decreases during yielding it will eventually become equal to the vertical stress. At this stage $p_i$ is equal to $K_a p_o$. Substitution of this value into Eqn.12 provides the extent $R_{tr}$ (for $\sigma_t = \sigma_v > \sigma_r$ and $\sigma_{vo}$).

Further reduction of the internal pressure (Stage (3)) will cause both the tangential and the vertical stress to decrease and arching will now occur in horizontal and vertical directions. Near the opening, where $\sigma_t = \sigma_v < p_o$, both modes of yielding (A and B) are evident. The extent of this zone is denoted by $R_{vr}$. Between $R_{vr}$ and $R_{tr}$, yielding is still governed by Mode A only and $R_{tr}$ can be estimated from Eqn.12. The extent of the plastic zone $R_{vr}$ (Modes A and B) is found by using the condition $\sigma_t = \sigma_v = p_o$ (i.e., Eqn.14 and 1):

$$R_{vr} = a(p_o/p_i)^{1/(N-1)} \ . \tag{15}$$

After propagation of yielding, the plastic zone contains a region where Mode A exists alone (Fig.5.a) and a region, close to the shaft, where Modes A and B occur simultaneously.

### 3.1.1.b) Initiation of Yielding by Mode B at $K_o < K_{cr}$ (Fig.6.a):

Fig.6.b shows the stress distributions in a horizontal section through the shaft at a particular depth in sequential stages of reducing the internal support pressure.

At Stage (1), yielding initiates at the wall in Mode B. The stress distributions are given by Eqns.1 to 3 and the internal

pressure is $p_i = \sigma_v/N = K_a p_o$ at yield initiation.

As $p_i$ is further reduced, $\sigma_t$ still increases due to wedging and $\sigma_v$ decreases due to vertical arching during downward displacement of the soil near the wall (Stage (2) in Fig. 6.b). Yielding propagates outward from the wall. The radial and tangential stress distributions are given by Eqns.2 and 3 until the stresses at the wall satisfy the failure criteria:

$$\sigma_t/\sigma_r = N \; . \tag{16}$$

The extent of the plastic zone due to the Mode B yielding at this stage is determined by equating radial stresses at the elastic/plastic interface for stress continuity. At this boundary, the radial stress in the elastic region is given by Eqn.2, and in the plastic zone by:

$$\sigma_r = \sigma_v/N \text{ and } \sigma_v = p_o \; . \tag{17}$$

Equating Eqns.2 and 17 yields:

$$R_{vr} = a\sqrt{[(K_o p_o - p_i)/(K_o - K_a)p_o]} \; . \tag{18}$$

At the end of Stage 2, the tangential stress becomes equal to the vertical stress and the support pressure is given by Eqn.11, or

$$p_i = 2K_o p_o/(N+1) \; . \tag{19}$$

Mode A is initiated at the wall.

Further relief of $p_i$, Stage (3), causes a simultaneous decrease of $\sigma_v$ and $\sigma_t$ (satisfying the failure criteria given by Eqns.16 and 17). At this stage, the maximum extent of the plastic zone ($R_{vr}$ in Fig.6.b) is still governed by Mode B-type yielding, but the radial stress distribution will differ from that in Eqn.2 because of the need to satisfy Eqn.16. Hence, in order to determine the radius of the plastic zone at this stage, the radial stress distribution needs to be calculated.

Fig.6.b, Stage (3), shows that inside the plastic zone
($r < R_{tr}$), where yielding in Mode A and B occurs ($\sigma_t = \sigma_v > \sigma_r$), the
radial and tangential stress distributions are (Ladanyi, 1974):

$$\sigma_r = p_i (r/a)^{N-1} \qquad (20)$$

$$\sigma_t = N p_i (r/a)^{N-1} \qquad (21)$$

if the influence of the vertical stress reduction is neglected.
The plastic zone $R_{tr}$ is as before (Eqn. 12):

$$R_{tr} = a[2K_o p_o/(N+1)p_i]^{1/(N-1)} . \qquad (22)$$

For the range $R_{tr} < r < R_{vr}$, the radial stress distribution
is governed by the stress equilibrium with the tangential stress:

$$\sigma_r = K_o p_o - (K_o p_o - \sigma_r')(R_{tr}/r)^2 \qquad (23)$$

where: $\sigma_r' = K_o p_o - (N-1)/(N+1)K_o p_o$ is the radial stress at
$r = R_{tr}$.

Substituting $r = R_{tr}$ and $\sigma_r'$ into Eqn.23 provides the radial
stress distribution in the outer plastic zone ($R_{tr} < r < R_{vr}$).
Continuity of radial stresses at the elastic zone boundary
($\sigma_r = K_a p_o$) locates the extent of the plastic zone, $R_{vr}$ as:

$$R_{vr} = a\sqrt{\{K_o[(N-1)/(N+1)][2K_o p_o/((N+1)p_i)]^{2/(N+1)}/(K_o - K_a)\}} . \qquad (24)$$

Again, after propagation of yielding, the plastic zone
contains a region where only one mode (Mode B) exists (Fig.5.b)
and a region, close to the shaft, where Mode A and B occur
simultaneously.

Eqns.1 to 24, are valid for conditions where horizontal
arching dominates. The influence of gravity was, so far,
neglected and will, in Section 3.2, be derived separately.

### 3.1.2 Wall Displacement ($u_i$)

Once the relationship between the support pressure and the extent of the plastic zone has been established, the corresponding wall displacement induced by stress relief can be determined. Some restrictive assumptions must be made to obtain a closed-form solution for the ground convergence curve ($p_i$-$u_i$-relationship). For horizontal arching, it is, as before, assumed that solutions for plane strain condition constitute a reasonable approximation, and that the radial wall convergence is due to changes in $\sigma_t$ and $\sigma_r$ only.

For the initial, elastic response, the wall displacements may be calculated using Lame's equation:

$$u_i = a[(K_o p_o - p_i)(1+\nu)]/E .  \tag{25}$$

After yielding is initiated, the wall displacement depends on the adopted constitutive model of the soil. Brown et al. (1983) presented a summary of currently available GCC formulations for different material models and for the idealistic case of a circular opening in an isotropic stress field under plane strain conditions. For simplicity, the displacements may be approximated by application of the solution proposed by Ladanyi (1974):

$$u_i = a\{1-[(1-e_{av})/(1+A_v)]^{1/2}\}  \tag{26}$$

where:  $e_{av}$ and $A_v$ are plastic dilation and deformation parameters defined by Ladanyi (1974).

This implies that the entire yield zone is treated as if Mode A would exist throughout. The extent of the plastic zone, needed for Eqn.26, is assumed to be given by the maximum extent described by Eqns.12 and 24, respectively.

## 3.2 Vertical Arching

### 3.2.1 Support Pressure

In the previous section, the support pressure was calculated to satisfy equilibrium in a horizontal plane only and vertical equilibrium was neglected. It has been shown that different types of yielding are induced if sufficient deformations due to radial stress relief are permitted . Three modes, A, B and C, have been identified for yield initiation and propagation (Figs. 1 and 5). For each mode, the plastic flow occurs along slip surfaces whose ultimate shear strength have been reached. The direction and shape of these failure surfaces differs for each mode as indicated on Fig.1. Since the shear resistance along these surfaces has been fully mobilized due to the far-field stresses, the soil mass tends to slide along these surfaces toward the shaft under its own weight. Consequently, to prevent instability, a support pressure, $p_g$, must be applied to the shaft wall in the area where gravity dominates. This phenomenon is referred to in this paper as 'gravity effect'. Vertical arching may, however, develop if sufficient vertical movement is permitted. From the orientation of the slip surfaces shown in Fig.1, it is evident, that gravity effects are more dominant in Modes A and B than in Mode C. In Mode C, sliding occurs in the tangential direction along spiral-shaped surfaces with no component in the radial direction.

As illustrated earlier, Fig.5, two zones of yielding containing one or both of two types of yield modes (A and/or B) are created if radial stress relief is permitted. Hence, two sets of slip surfaces exist in the inner zone near the shaft wall and only one set in the outer zone. Sliding along any set of slip surfaces could occur due to gravity. However, unstable blocks tending to slide inward toward the shaft opening must be bounded by two sets of slip surfaces for a kinematically possible failure mode. This condition is satisfied when Mode A and B occur simultaneously. In the outer zone, for Mode A-types yielding,

only vertical sliding along spiral-shaped surfaces is possible without overcoming additional resistances. No radial sliding component exists. For the case of Mode B-type yielding (in the outer zone), the inclined slip surfaces are formed initially but blocks are prevented from sliding inward due to wedging action and because the ultimate strength has not yet been reached for tangential loading. The gravitational support pressure $p_g$, required to prevent instability therefore arises only from the inner zone with two sets of slip surfaces. Nevertheless, because of the close proximity of the state of stress in the outer zone to the failure state, the gravitational support pressure is calculated in this paper based on the maximum extent for both zones.

This support pressure, $p_g$, can be determined by application of one of two classical approaches: (1) limit state equilibrium (LEM) and (2) plastic equilibrium (PEM). Prater (1977) adopted the first approach to calculate the support pressure required to prevent initiation of sliding along conical failure surfaces without considering the influence of horizontal arching. The influence of yield propagation, the effect of the extent of the yield zone and the related stress redistribution were not included in this approach. Consequently, the total support pressure could not be correctly determined.

The second approach has commonly been used to determine the lateral pressure exerted by a flowing mass, e.g., for horizontal stress determination in silos (Kendal, 1980). Handy (1984) applied this approach after some adjustment for soil/wall interaction to estimate the lateral pressures on retaining walls, and demonstrated satisfactory agreement with results from model tests. The conditions near a shaft resemble those near a retaining wall. Hence, the plastic equilibrium approach is adopted in the following to calculate the total support pressure, $p_g$. This pressure is determined by assuming that slip surfaces were created by horizontal arching. It represents the total support pressure required to maintain stability.

Fig. 7 shows the forces acting on a horizontal soil element within the yield zone. Summation of the vertical stresses, assumed to be uniform, acting on the element leads to:

$$d\sigma_v = [\gamma - \frac{2\pi\sigma_v}{A} (\frac{K_s\mu_s R}{\sin a} + K_w\mu_w a)] \, dh \qquad (27)$$

where:  A  = sectional area of the yield zone (= $\pi(R-a)^2$);

  $a$  = angle to the inclined yield surface ($a$ = 90° for Mode A; $a$ = 45° + $\phi/2$ for Mode B);

  $K_s$  = stress ratio at wall/soil interface (=$K_a$);

  $\mu_s$  = frictional coefficient at soil/soil interface; and

  $\mu_w$  = frictional coefficient at soil/wall interface.

Integration of Eqn.27 provides the vertical stress, $\sigma_v$, distribution with depth, and the total horizontal pressure required to prevent instability is thus given by the plastic equilibrium condition:

$$p_g = K_a \, \sigma_v \, . \qquad (28)$$

An example is presented in the following section.

Eqns. 27 and 28 show that the support pressure, $p_g$, increased with increasing extent of yield zone, R. For a given size of yield zone, this pressure induced by Mode A-type yielding is higher than that by Mode B because of differences in the orientation of the shear plane (i.e., $a$). Hence, if two zones of different yielding mode occur, $p_g$ is governed by the outer yield zone radius for Mode A yield initiation while the radius of the inner yield zone dominates design for Mode B yield initiation because this zone has a steeper boundary (larger $a$) and thus a greater gravity effect.

Eqns.27 and 28 are applicable only for cohesionless soils. The gravity effect in cohesive soils differs because the shear strength of cohesive soils is independent of confining pressure.

This case is presented in Appendix C.

## 3.2.2 Displacements near the Shaft Collar

A solution for displacements considering gravity is not available and it is recommended, as a first approximation, to neglect gravity for the prediction of wall displacements and to determine the convergence using the approach given in Section 3.1.2.

The extent of the yield zone near the ground surface can be used as an indicator of the width of the surface settlement trough.

## 3.4 Summary of Design Procedure Based on Convergence/Confinement Method

It is suggested that the behaviour of a shaft can be described and treated by independently considering horizontal and vertical arching near the shaft. These two arching actions can be quantified by use of the CCM with inclusion of gravity effects. In this fashion, it is possible to derive a relationship between the support pressure and the radial displacement. The CCM for shaft design consists of the following steps (refer to Fig.8):

1. Identify the mode of yielding near the shaft wall. It depends on the initial in-situ stress $(K_0)$; it governs the extent of the plastic zone and the shape of convergence curve.

2. Calculate the ground convergence curves for a specific elevation $h_i$ and determine the extent of the plastic zone, using the appropriate two-dimensional model (Fig.8.a). Neglect gravity effects.

3. Select a specific wall displacement, $u_s$, based on a serviceability design criteria and establish pressure versus depth and plastic zone versus depth relationships from results of Step 2 (Fig.8.b and Fig.8.c; full line).

4.  With the configuration of the plastic zone around the shaft,
    determine the gravitational support pressure distribution,
    $p_g$, with depth (Fig.8.c; dashed line).

5.  To the two pressure distributions due to horizontal (full
    line) and vertical (dashed line) arching form an envelope of
    required support pressure (Fig.8.c; shaded) for the specified
    wall displacement $u_s$.

6.  Adjust the pressure envelope at the bottom of the shaft for
    the reduced pressure caused by face effects (Panet and
    Guenot, 1982).

7.  Multiply pressure envelope by appropriate load factor to
    arrive at a design envelope. The resulting pressure should be
    checked as not to exceed pressure at rest.

It follows from the above calculation steps that the
resulting design pressure distribution envelope depends on an
assessment of acceptable ground movements.


## PART II - VERIFICATION OF DESIGN METHOD

## 4. COMPARISON OF PROPOSED SOLUTION WITH NUMERICAL SIMULATION

The numerical examples generated by application of the
finite element method (FEM) are intended to compare results with
the proposed method. They are not designed to simulate any
particular case history but are aimed at illustrating mechanisms
of typical shaft behaviour. For example, the magnitudes of $K_o$
were chosen to represent two extreme conditions ($K_o < K_{cr}$ and $K_o
> K_{cr}$) and create two difference modes of yielding.

## 4.1 Finite Element Analyses

The finite element program SAFE, developed at the University of Alberta by Chan (1985), was used for this comparison. The soil near the shaft was discretized for an axisymmetric shaft by pie-shaped elements. The configuration of the mesh, consisting of 8-node quadrilateral iso-parametric elements, is shown in Fig.9. Zero displacement boundary conditions were assumed at three boundaries (AB, BC, and CD) for the initial stress determination by 'switch on gravity'. The Boundary AB, representing the wall of a 2 m diameter shaft, was then allowed to move inward to simulate shaft construction. The specified displacement profiles is shown in Fig.9. It enforces a constant wall displacement ($u_i$) along the shaft except near the base.

Three analyses were performed to investigate the shaft behaviour in purely cohesionless and cohesive soils. For cohesionless soil, an elastic, perfectly plastic model and the Mohr-Coulomb yield criteria with associated flow rule was used and a set of typical soil parameters were selected (Table 1). Two $K_o$-values, 0.409 and 0.980, were chosen to create two typical modes of yielding.

Because of the assumed associated flow rule for the cohesionless soil, deformations due to dilation and, hence, arching effects will be exaggerated as compared to what might be expected in reality. For cohesive soil, the unconfined compression strength of the ground was assumed to be constant with depth and the elastic, perfectly plastic model with the von-Mises yield criteria with no volume change was employed.

A minimal surcharge (equivalent to 3 or 4 meters of cohesionless or cohesive soil, respectively) was applied at the ground surface, to overcome the problem of yielding at zero confinement near the ground surface. Some numerical convergence problems were experienced. This is commonly encountered in FEM-analysis involving non-linearity, plasticity near the limit

equilibrium state (Borst and Vermer, 1984, and Griffiths and Koutsabeloulis, 1985). The incremental displacement step after formation of a plastic zone was selected at u/a=0.01% resulting in 4 to 10 iterations for reasonable convergence tolerances.

## 4.2 Results from Finite Element Analysis

### 4.2.1 Stress Distribution

The radial, tangential and vertical stress distributions around the shaft after the final displacement step are plotted in Figs. 10 to 12 for three soil or stress conditions. Yielding has occurred in all cases. In Case SM1 (Fig.10), yielding was induced by Mode B, and the tangential stresss is always the intermediate stress during propagation. In contrast, in Cases SM2 and CM1, Mode A governs the yield initiation and the vertical stress is always the intermediate stress. However, the stress distribution patterns are similar for the three cases, except near the lower boundary. The radial stress decreases toward the shaft wall because of stress relief and causes stress redistribution as horizontal arching develops. The tangential stresses initially increase in the elastic and plastic regions but decreases during yield propagation close to the shaft.

The drastic reduction of vertical stresses near the shaft wall indicates that arching in vertical planes near the elastic/plastic interface develops in all cases (the shaft wall friction is zero). As a consequence, a slight increase of the vertical stress is observed at the interface.

The stress distributions at one horizontal section (depth h=3.8m) for Case SM 2 is plotted in Fig.13 for comparison with stresses calculated by the CCM. This particular section is remote from the ground surface and the shaft bottom. Stress distributions at two displacement stages are plotted: first, when yielding at the wall is initiated (at u/a=0.26%) and, second, after much yielding has occurred. The results in Fig.13 indicate that yield initiation occurred in Mode A, as expected. The stress

distributions predictedj by the CCM agrees well with those from the FEM.

## 4.2.2 Radial Displacement and Plastic Zone Radius Development

Figs. 14 to 16 present results of the radial support pressure/wall displacement and support pressure/plastic zone radius relationships obtained from the FE analyses (designated by crosses) and by the CCM (full lines). The numbers on the GCC plot $(p_i - u_i)$ correspond to the different stress stages described in Figs. 4 and 6. In Zone 1, the ground responds elastically; Line E separates elastic from plastic behaviour. Beyond Line E yielding is induced for SM1 (Fig.14) by Mode B, and this results in a non-linear response curve. Further stress relief causes a reduction of the tangential stress near the wall until it becomes equal to $\sigma_v$. This state is represented by Line T.

For Cases SM2 and CM1, the mode of yielding differs, i.e., initiation by Mode A. Lines E and T in Case CM1 are parallel and vertical because yielding in purely cohesive soil is induced at a constant stress difference equal to the compressive strength of the soil.

The $p_i - R$ plots demonstrate outward propagation of the plastic zone due to support pressure reduction. The results predicted by the CCM agree reasonably well with those of the FE analyses.

## 4.2.3 Extent of Plastic Zone with Depth

The extent of the plastic zone in a vertical section at two displacement levels obtained by both methods, FEM and CCM, is presented in Fig.17. Because of the coarseness of the FE mesh, the extent varies in a steplike fashion for the FE analysis but the results of the two methods agree well, considering that yielding is only indicated at the inegration points of each element. For the enforced wall displacement profile (Fig. 9), the radius of the plastic zone decreases with depth for cohesionless

soils and forms a cone whereas it is constant for a shaft in cohesive soils, forming a cylinder (above a short cone). In cohesionless soils, at the same displacement, a larger plastic zone develops for Case SM1 at lower field stress ($K_0=0.41$). This implies that the pressure due to gravity in Case SM1 ($K_0<K_{cr}$) is more dominant than in Case SM2 ($K_0>K_{cr}$). However, the support pressure at a fixed deformation level is greater in Case SM2 because of higher in situ stress (see Fig.18).

## 4.2.4 Pressure Distribution at Wall

From the GCCs (Figs. 14 to 16), the support pressures required to maintain equilibrium at a given displacement are plotted on Fig.18 for three displacements levels together with results from the FE analysis. Both methods give consistent results except at the bottom boundary. These figures clearly show that the support pressure is a function of wall displacement and in situ stress. Pressures predicted by the CCM for $u/a=0.8\%$, i.e., 8mm wall movement, are shown on Fig.18. The support pressure determined from the limit equilibrium method proposed by Beresantzev (1958) is included for comparison. Large displacements would have to be allowed in order to obtain these minimum pressures.

The support pressure for a constant wall displacement increases steadily with depth for all three cases, even at $h/a > 4$ where the methods by Terzaghi (1943) and Berezantzev (1958) predict constant minimum support pressures. The rapid increase at a depth of more than 6m is an artifact of the enforced displacement distribution near the shaft bottom.

Gravity effects and vertical arching within the plastic zone around the shaft was not dominant in these cases because relatively small displacements ($u/a$ = 0.3 to 0.56%) were imposed. Large movements could not be simulated because of convergence problems. Nevertheless, the CCM provides an excellent tool to predict the ground pressure at specified, large displacement

levels.

## 4.3 Gravity Effect and Vertical Arching

Because of difficulties in simulating behaviour at large
displacements by FE analysis, several analytical examples have
been generated to illustrate the role of gravity for shaft
design. Results determined by application of Eqns.27, 28 and C.1
for cohesionless and cohesive soils are plotted in Figs. 19 and
20. Dimensions of the shaft and the shape as well as the extent
of the assumed plastic zone are also shown.

Fig.19 indicates that for cohesionless soil, the support
pressure due to gravity effect increases as the yield zone
expands. The distribution of the support pressures depends
heavily on the assumed configuration of the plastic zone. It
reduces to zero at depth for cone shaped plastic zones. For
cylindrical yield zones, as assumed by Terzaghi (1943), a
constant pressure would be approached. Near the surface, the
pressure is close to the active earth pressure.

In cohesive soil (Fig.20), the support pressure to prevent
instability due to gravity also increases for larger yield zones.
However, a distinct difference in vertical arching action exists
between cohesionless and cohesive soils. For cohesive soils,
support pressure applied along the upper portion of the shaft
does not enhance the stability because the shear strength of the
cohesive soil is independent of the confining pressure. The
support pressure to inhibit collapse must be applied where a
collapse mechanism is possible, generally near the bottom (Britto
and Kusakabe, 1983).

Combining Fig. 18 and 19 provides the expected pressure
distribution for Case SM1 (Fig. 21). Near the collar, to about 5m
depth, gravity dominates. Below this level the pressure is
displacement controlled (shown for $u/a \geq 0.5\%$). Because this
pressure represents the actually expected pressure, a load
factored pressure should be used for design of the shaft lining.

The load factor should, however, be selected so that the resulting design pressure does not exceed the stress at rest.

## 5. DISCUSSION

### 5.1 Horizontal versus Vertical Arching

Stress relief due to the shaft excavation causes horizontal and vertical arching near a shaft. It is of practical importance to understand under what conditions horizontal or vertical arching dominates shaft behaviour and becomes relevant for design. The CCM provides an effective tool to depict the role of each type of arching quantitatively. Fig. 22 presents a schematic GCC with the support pressure normalized to initial state of stress $(K_o p_o)$. This reduces the GCC for different elevations to one unique curve, if horizontal arching is considered only and gravity is neglected. The normalized support pressure due to gravity, $(p_g/K_o p_o)$, during vertical arching is sketched for two depths; for a section close to the surface (shallow) and for a level at greater depth (deep). This diagram illustrates two features of practical significance: (1) horizontal arching prevails for small wall displacements, i.e., when good ground control is exercised, and at greater depths; and (2) vertical arching and, hence, gravity effects dominate only when 'excessive' yielding is permitted and only at shallow depth.

It follows then, that previously proposed design methods are seldom in agreement with modern construction procedures and design requirements enforcing good ground control to minimize surface settlement and ground disturbance.

### 5.2 Limitations of the Proposed Approach

Many assumptions had to be made to arrive at closed-form solutions for the CCM. It is imperative to investigate for practical applications how these assumptions and approximations affect the accuracy of the results. For the simulation of horizontal arching, the 2-D plane stain 'hole-in-plate' model was

employed. The neglectance of shear stresses between horizontal layers, whose effect have been investigated in detail by Terzaghi (1943), could lead to an underestimation of the extent of the yield zone, and thus a slightly unconservative support pressure. This was already recognized by Terzaghi who recommended to use a reduced friction angle for compensation (see Section 2.1). It must be realized that the assumed 2-D plane strain condition does not prevail at shallow depth where the gravity effect dominates. However, horizontal arching normally initiates yielding near the surface and, hence, correctly reflects the true shaft behaviour before gravity dominates. At greater depth, the model is a reasonable approximation for all displacement levels and distributions.

For the calculation of the support pressure to resist gravity, the vertical stress distribution is assumed to be uniform at each depth. This assumption is contradicted by the results of the finite element analyses which demonstrate that the vertical stress increases rapidly away from the shaft wall. Thus the assumption of a constant average $\sigma_v$ results in a higher (conservative) support pressure $p_g$ due to gravity effects (Eqns. 27 and 28). The existance of shear stresses causes a rotation of the yield plane (i.e., a reduction of the angle $a$ in Eqn. 27), and neglectance of this effect leads to a conservative estimate of $p_g$.

## 5.3 Effect of Variation of E and $q_u$ with Depth on Shape of Plastic Zone

For the previously presented analyses, Young's modulus, E and shear strength, $q_u$, were assumed to be independent of depth. This assumption may not be valid in practice. Equations governing the extent of the plastic zone depend on these parameters. Consequently, shape and extent of the plastic zone must be affected by this simplification. This effect has been studied by Wong (1986) and revealed the following:

## a) Cohesionless Soils

For a constant modulus, the extent of the yield zone can be determined as a function of depth using Eqn.12 and Eqns.18 and 24 for Modes A and B, respectively. For Mode A and a constant imposed shaft wall displacement, yielding occurs on vertical (spiral) surfaces and its extent decreases rapidly with the depth. For Mode B, yielding caused by the vertical-radial stress difference occurs along inclined (conical) surfaces following the Rankine's slip lines and its configuration looks like the truncated cone assumed by Prater (1977).

For soils with a linearly increasing modulus with depth, the profile of the yield zone will look as shown in Fig. 23. With a constant wall displacement imposed, the magnitude of stress relief with depth is larger and the extent of the yield zone is greater at depth.

Fig. 23 shows that cone-shaped yield zones may develop in cohesionless soils. Hence, the method proposed by Berezartzev (1958) seems appropriate for the determination of the minimum support pressure requirement but for conditions of constant soil stiffness only.

## b) Cohesive Soils

Similar reasonings as for cohesionless soils are applicable to cohesive soils. Equations governing the shape of the yield zones for Modes A and B are given in Appendix B (Eqn. B.12 and Eqns. B.18 to B. 24 respectively). Fig. 23 illustrates possible configurations of the plastic zones for different cases. The plastic zone may be cone-shaped or cylindrical depending on the strength and deformation property variation with depth. The extent of the plastic zone generally diminishes rapidly at the bottom of the shaft because of the face effect.

Britto and Kusakabe (1982, 1983) investigated the mechanism of the collapse modes of unsupported axi-symmetric excavations in

soft clays theoretically and experimentally. Their findings agree
well with the shapes shown in Fig. 23.

## 6. CONCLUSIONS

The behaviour of shafts in cohesionless and cohesive soils,
including the transition from elastic repsonse to yielding and to
collapse, has been explored in detail. It depends on the mode of
yield initiation and propagation and the influence of gravity.
Stability of a shaft is enhanced by two types of arching,
horizontal and vertical, that develop around a shaft opening if
sufficient wall displacements are permitted during construction.
It was found that in cohesionless soils horizontal arching
prevails at small wall displacements and at great depth whereas
vertical arching is only mobilized after large displacements and
near the ground surface. For cohesive soils, when a distinct
collapse mechanism is established, the support pressure required
to prevent the instability arises primarily from gravity effects
but yielding is caused and controlled by horizontal arching.

It is suggested that horizontal and vertical arching can be
approximately quantified by application of the
Convergencement/Confinement Method with consideration of gravity
effects. This method provides a performance prediction model
which predicts required support pressures with respect to
displacement or serviceability design criteria. It differs from
conventional approaches in which the limit state of equilibrium
is considered and, hence, reasonable safety margins must be
selected carefully. The new design method has been verified in
this paper by comparison with results from finite element
simulations. The method provides reliable estimates of support
pressure, wall displacement and extent of plastic zone. It
constitutes a rational design method as well as an approach for
performance prediction and assessment of field measurements. Its
validity was also verified by comparison with measurements from
case histories. This will be published in a future paper.

The proposed design method provides support pressure distribution with depth for specified wall displacements. Hence, it was possible to evaluate the limits of applicability of conventional design methods. These methods generally provide minimum support pressures required to prevent collapse. These values can, however, only be reached if the wall displacements are large and for most practical purposes excessive and unacceptable.

## 7. ACKNOWLEDGMENTS

## 8. REFERENCES

Abel, J.F., Dowis, E. and Richards, P., 1979. Concrete shaft lining design. 20th U.S. Symposium on Rock Mechanics, Austin, Texas, pp. 627-633.

Berezantzev, V.G., 1958. Earth pressure on the cylindrical retaining walls. Conference on Earth Pressure Problems, Brussels, II, pp.21-24.

Britto, A.M. and Kusakabe, O., 1982. Stability of axisymmetric excavations. Geotechnique, 32, pp.261-270.

Britto, A.M. and Kusakabe, O., 1983. Stability of axisymmetric excavations in clays. Journal of Geotechnical Engineering, ASCE, 109, pp.666-681.

Britto, A.M. and Kusakabe, O., 1984. On the stability of supported excavations. Canadian Geotechnical Journal, 21, pp.338-348.

Brown, E.T., Bray, J.W., Ladanyi, B. and Hoek, E., 1983. Ground response curves for rock tunnels. Journal of Geotechnical Engineering, 109, pp.12-23.

Chan, D., 1985. Finite Element Analysis of Strain-softening Materials. Ph.D. Thesis. Dept. of Civil Enginnering, University of Alberta, Edmonton, Alberta, 355p.

De Borst, R. and Vermeer, 1984. Possibility and limitations of finite element for limit analysis. Geotechnique, 34, pp.199-210.

Fenner, R., 1939. Untersuchungen zur Erkenntnis des Gebirgsdruckes. Glueckauf, Ann. 74:32,33.

Griffiths, D.V. and Koutsabeloulis, N., 1985. Discussion on 'Possibility and limitations of finite element for limit analysis', Geotechnique, 35, pp.90-94.

Handy, R.L., 1985. The arch in soil arching. Journal of
    Geotechnical Engineering, ASCE, 111, pp.302-319.

Kendal, N.O., 1980. The practical design of silo and bunkers with
    reference to the Codes of Practice. International Conference
    on Design of Silos for Strength and Flow, Session 6,
    University of Lancaster, U.K., 29p.

Ladanyi, B., 1974. Use of the long-term strength concept in the
    determination of ground pressure on tunnel linings. Advances
    in Rock Mechanics; Third Congress of the International
    Society for Rock Mechanics, 2.B, pp.1150-1156.

Lade, P.V., Jessberger, H.L., Makowski, E. and Jorden, P., 1981.
    Modelling of deep shaft in centrifuge tests. 10th
    International Conference on Soil Mechanics and Foundation
    Engineering, 1, pp.683-642.

McCreath, D.R., 1980. Analysis of Formation Pressure on Tunnel
    and Shaft Linings. M.Eng. Report, Department of Civil
    Engineering, University of Alberta, Edmonton, Alberta, 73p.

Müller-Kirchenbauer, H., Walz, B., and Klapperich, H., 1980.
    Experimentelle und Theoretische Untersuchungen zum
    Erddruckproblem auf Radial Symmetrische Senkkästen und
    Schächte, Berlin, 113p.

Pacher, F., 1964. Measurements of deformations in a test gallery
    as a means of investigating the behaviour of the rock mass
    and specifying lining requirements. Rock Mechanics and
    Engineering Geology, Supplement I, pp.149-161.

Panet, M. and Guenot, A., 1982. Analysis of convergence behind
    the face of a tunnel. Tunnelling'82, The Institution of
    Mining and Metallurgy, pp.197-204.

Prater, E.G., 1977. An examination of some theories of earth
    pressure on shaft linings. Cananadian Geotechnical Journal,
    14, pp.91-107.

Terzaghi, K., 1943. Theoretical Soil Mechanics. John Wiley and
    Sons, 502p.

Wong, R.C.K. and Kaiser, P.K.K., 1984. Interpretation of
    Measurement on Tunnel in Clay Shale and Shaft in Edmonton
    Till. Report submitted to Department of Water and Sanitation,
    City of Edmonton, and the AOSTRA, 277p.

Wong, R.C.K., 1986. Design and Performance Evaluation of Tunnels
    and Shafts. Department of Civil Engineering, University of
    Alberta, Ph.D. thesis, 308p.

# APPENDICES

Appendix A - Notation

Appendix B - Mechanism of Shaft Behaviour in Cohesive Soil

Appendix C - Gravity Effect in Cohesive Soil

Appendix A

**Notation**

a          = radius of shaft

H         = depth of shaft

h         = depth measured from ground surface

A         = area of cross section

R         = radius of plastic zone

$R_{tr}$    = radius of plastic zone induced by tangential/radial stress difference (Mode A)

$R_{vr}$    = radius of plastic zone induced by vertical/radial stress difference (Mode B)

r         = radial distance

$u_i$      = radial displacement of shaft wall (at r=a)

$\sigma_r$      = radial stress

$\sigma_v$      = vertical stress

$\sigma_t$      = tangential stress

$\sigma_1, \sigma_3$  = major and minor principal stress

$\tau$        = shear stress

$\sigma_h$      = minor horizontal stress

$\sigma_H$      = major horizontal stress

$p_i = p_s$  = internal or support pressure (radial stress) at wall

$p_o$      = vertical initial in-situ stress

$p_g$      = stress due to gravity effect

$\gamma$        = unit weight of soil ($=\rho g$)

$\rho$        = density of soil

$\nu$        = Poisson's ratio

E         = Young's modulus

$e_{av}$     = average plastic dilation

$A_v$ = parameter for calculating plastic deformation

$\phi$ = angle of internal friction of soil

$N$ = $\tan^2 (45° + \phi/2)$

$q_u$ = unconfined compression strength of cohesive soil

$c_u$ = shear strength of cohesive soil

$\mu_w$ = wall friction coefficient

$\mu_s$ = soil friction coefficient

$K = \lambda$ = ratio of horizontal to vertical stress

$K_s$ = K at soil/soil boundary

$K_w$ = K at soil/wall boundary

$K_o$ = K at rest

$K_a$ = K in active state ( = $\tan^2(45°-\phi/2)$

$K_{cr}$ = critical K-value distinguishing Mode A from Mode B

APPENDIX B

## Mechanism of Shaft Behaviour in Cohesive Soil

This appendix contains the equations governing shaft behaviour in cohesive soils. Equations are designated in the same sequence as those for cohesionless soil. Thus, explanations given in the main text for cohesionless soils are generally applicable to this appendix. Notations are given in Appendix A.

The stresses in an elastic thick walled hollow cylinder are:

$$\sigma_v = \gamma h = p_o \tag{B.1}$$

$$\sigma_r = K_o p_o - [K_o p_o - p_i](a/r)^2 \tag{B.2}$$

$$\sigma_t = K_o p_o + [K_o p_o - p_i](a/r)^2 \tag{B.3}$$

For a cohesive material the strength is assumed to be constant:

$$(\sigma_1 - \sigma_3) = q_u \tag{B.4}$$

Hence, the support pressures for the three possible modes of yield initiation are:

$$\text{For Mode A: } p_i = K_o p_o - q_u/2 \tag{B.5}$$

$$\text{For Mode B: } p_i = p_o - q_u \tag{B.6}$$

$$\text{For Mode C: } p_i = (2K_o - 1)p_o - q_u \tag{B.7}$$

The largest value of $p_i$ will govern the mode of yield initiation. This can be expressed in terms of required $K_o$-values:

$$\text{Mode A: } [1 - q_u/(2p_o)] < K_o < [q_u/(2p_o) + 1] \tag{B.8}$$

$$\text{Mode B: } K_o < [1 - q_u/(2p_o)] \tag{B.9}$$

$$\text{Mode C: } K_o > [q_u/(2p_o)+1] \tag{B.10}$$

As for cohesionless soils, Mode C has been neglected in the following analysis. A critical K-value, $K_{cr}$, is used to distinguish Mode A from Mode B:

a) **Mode A** $(\sigma_t - \sigma_r)$ **at** $K_o > K_{cr}$

The yielding initiates at the condition of:

$$(\sigma_t - \sigma_r) = 2K_o p_o - 2p_i = q_u \tag{B.11}$$

A further decrease in the support pressure causes a propagation of a plastic zone to:

$$R_{tr} = a\{\exp[(K_o p_o - p_i)/q_u - 1/2]\} \tag{B.12}$$

Stresses within the plastic zone $R_{tr}$ are:

$$\sigma_r = p_i + q_u \ln(r/a) \tag{B.13}$$

$$\sigma_t = p_i + q_u [1 + \ln(r/a)] \tag{B.14}$$

Additional stress relief causes yielding in Mode B (together with Mode A) and the extent of this zone, $R_{vr}$, is:

$$R_{vr} = a \exp[(p_i - p_o)/q_u] \tag{B.15}$$

b) **Mode B** $(\sigma_v - \sigma_r)$ **at** $K_o < K_{cr}$

Yielding initiates at:

$$p_i = \sigma_v - q_u \tag{B.16}$$

As $p_i$ is further reduced, the vertical stress decreases due to the vertical arching and the tangential stress will increase until it becomes equal to the vertical stress at the wall. At this state, the radial stress at the elastic/plastic boundary is given by:

$$\sigma_r = \sigma_v - q_u \text{ and } \sigma_v = p_o. \tag{B.17}$$

Equating this stress with that in the elastic zone given by Eqn.B.2 provides the radius of the plastic zone:

$$R_{vr} = a\sqrt{\{(K_o p_o - p_i)/[(K_o-1)p_o + q_u]\}} \tag{B.18}$$

and the support pressure is:

$$p_i = (K_o p_o - q_u/2) \tag{B.19}$$

Further relief in support pressure causes propagation of the plastic zone. The mode of yielding is still Mode B. But near the shaft wall, there exists a zone where the tangential stress is equal to the vertical stress. Within this zone, the radial and tangential stresses, governed by the failure criteria, are given as Ladanyi (1974):

$$\sigma_r = p_i + q_u \ln(r/a) \tag{B.20}$$

$$\sigma_t = p_i + q_u(1+\ln(r/a)) \tag{B.21}$$

and the extent of this zone is:

$$R_{tr} = a\{\exp[(K_o p_o - p_i)/q_u - 1/2]\} \tag{B.22}$$

The radial stress distribution in the zone of Mode B yielding must be known for the determination of the extent of the plastic zone. Between $R_{tr} < r < R_{vr}$ (shown in Fig.6.b), conditions of equilibrium provide the radial stress:

$$\sigma_r = K_o p_o - [(K_o p_o - \sigma_r')(R_{tr}/r)^2] \tag{B.23}$$

where: $\sigma_r' = 2K_o p_o - q_u$ at $r = R_{tr}$.

Substituting $r = R_{tr}$ and $\sigma_r'$ into Eqn.B.23 yields the radial stress distribution in the plastic zone ($R_{tr} < r < R_{vr}$). Continuity of radial stresses at the elastic zone boundary ($\sigma_r = K_a \sigma_v$) locates the extent of the plastic zone, $R_{vr}$ as:

$$R_{vr} = a\sqrt{\{(K_o p_o - q_u) \exp[2((K_o p_o - p_i)/q_u - 1/2)]/[(1-K_o)p_o + q_u]\}} \quad \text{(B.24)}$$

The wall displacements are calculated based on the model proposed by Ladanyi (1974). For elastic ground response, the wall displacement is:

$$u_i = a[(K_o p_o - p_i)(1+\nu)]/E \quad \text{(B.25)}$$

If yielding occurs, the displacements are:

$$u_i = a\{1 - [1/(1+A_v)]^{1/2}\} \quad \text{(B.26)}$$

APPENDIX C


Gravity Effect and Vertical Arching in Cohesive Soils


The shear resistance of cohesive materials is independent of confining pressure. Hence, applying horizontal pressure on the shaft wall does not enhance the strength of the soil in the plastic zone. Hence, it is necessary to identify possible collapse mechanisms and to inhibit these by application of external forces.

Fig.C.1 shows one possible collapse mechanism. The cylindrical plastic zone will cave in (slide vertically) and exert a force, W', on the conical soil mass underneath. A horizontal pressure must be applied to inhibit failure of this soil cone. The required total force, $P_g$, is given by considering the force equilibrium along the inclined failure surface of the conical soil mass:

$$(W' + W_c)\sin a - P_g(\cos a) - F_c = 0 \qquad (C.1)$$

Behaviour of Vertical Shafts

Parts III: Evaluation of Model Test Results
Part IV: Evaluation of Case Histories

by

R.C.K. Wong* and P.K. Kaiser**

*ESSO Resources Canada Ltd.
Calgary, Alberta
**Professor of Civil Engineering
Department of Civil Engineering
University of Alberta
Edmonton, Canada, T6G 2G7
(403) 432-5106

# ABSTRACT

Wong and Kaiser (1987; Part I) proposed the use of Convergence/Confinement Method with the inclusion of gravity effects as an analytical tool to predict the behaviour of vertical shafts. In this paper, results from this method are compared with measurements to evaluate the performance of several instrumented, full scale and model shafts. This evaluation confirms that the proposed method provides satisfactory predictions of shaft behaviour in various soil types (i.e., support pressure/radial displacement relationship). It is also shown that the actual support pressures, monitored in the model test and in the field, are higher than those predicted by the conventional design methods. Practical implications are discussed.
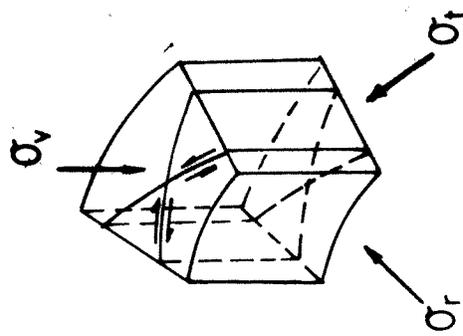
$signoff

(a) Mode 'A'
$(\sigma_t - \sigma_r) = $ max.

(b) Mode 'B'
$(\sigma_v - \sigma_r) = $ max.

(c) Mode 'C'
$(\sigma_t - \sigma_v) = $ max.

Wong and Kaiser (I+II) Fig. 1

- Y-axis: $\frac{H}{a}$ (values 0 through 10)
- X-axis: $p_s / a\gamma$ (0.00, 0.25, 0.50, 0.75, 1.00)

$\phi_p = 30°$
$C = 0$
$\gamma = 20\ KN/M^3$

$K_o \gamma h$

$K_a \gamma h$

Prater:
$\lambda = K_o$
$= 1 - \sin\phi$

Berezantzev

Terzaghi

$K_oP_o$

$K_oP_o$

$P_i$

R

1 - 1

(a) HORIZONTAL ARCHING

a

$P_i$

1

1

Plastic
Zone
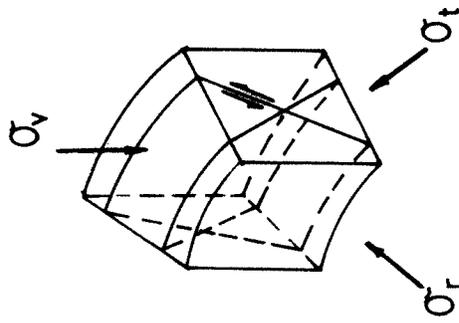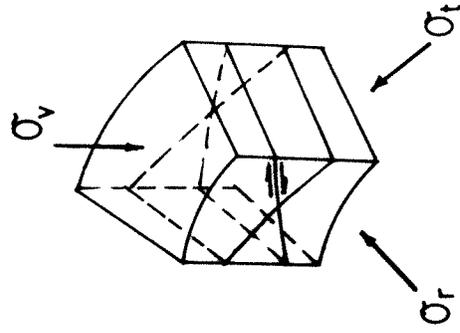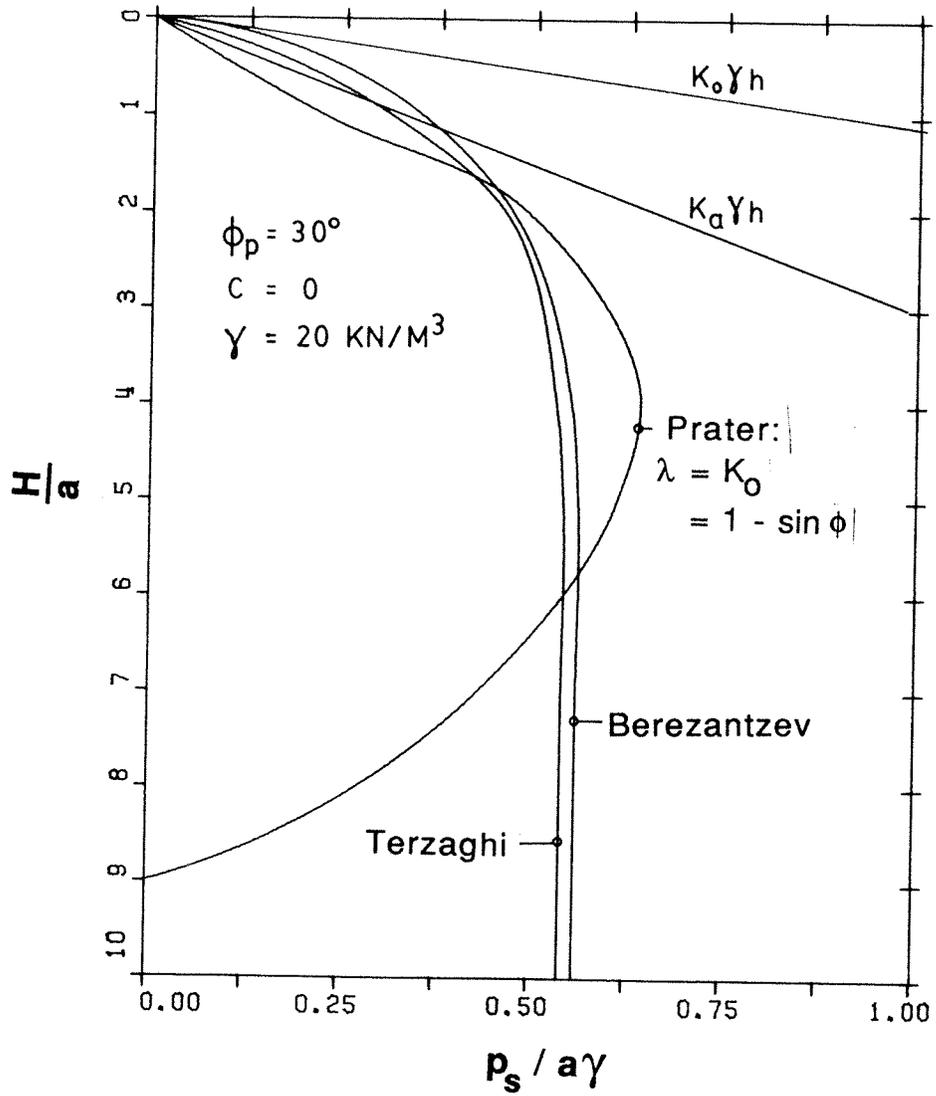
(b) VERTICAL ARCHING

Wong and Kaiser (I+II) Fig. 3
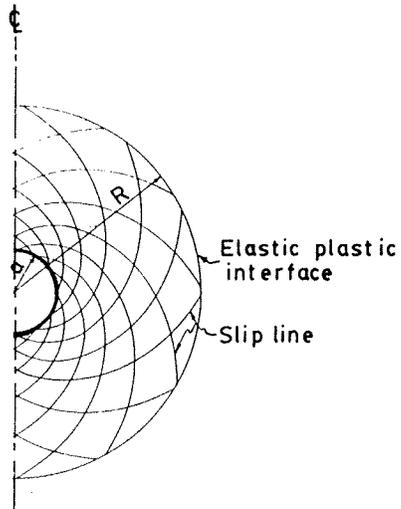
(a) MODE A
    ( $K_o > K_{cr}$ )

| Stress Distribution around opening | Stress State at shaft wall |
|---|---|
| (1) | |
| (2) | |
| (3) | |

(b)

Wong and Kaiser (I+II) Fig. 4

(a) $K_o > K_{cr}$

(b) $K_o < K_{cr}$

Slip line

Elastic-plastic interface

$\alpha = 45° + \phi/2$

(a) MODE B
($K_o < K_{cr}$)

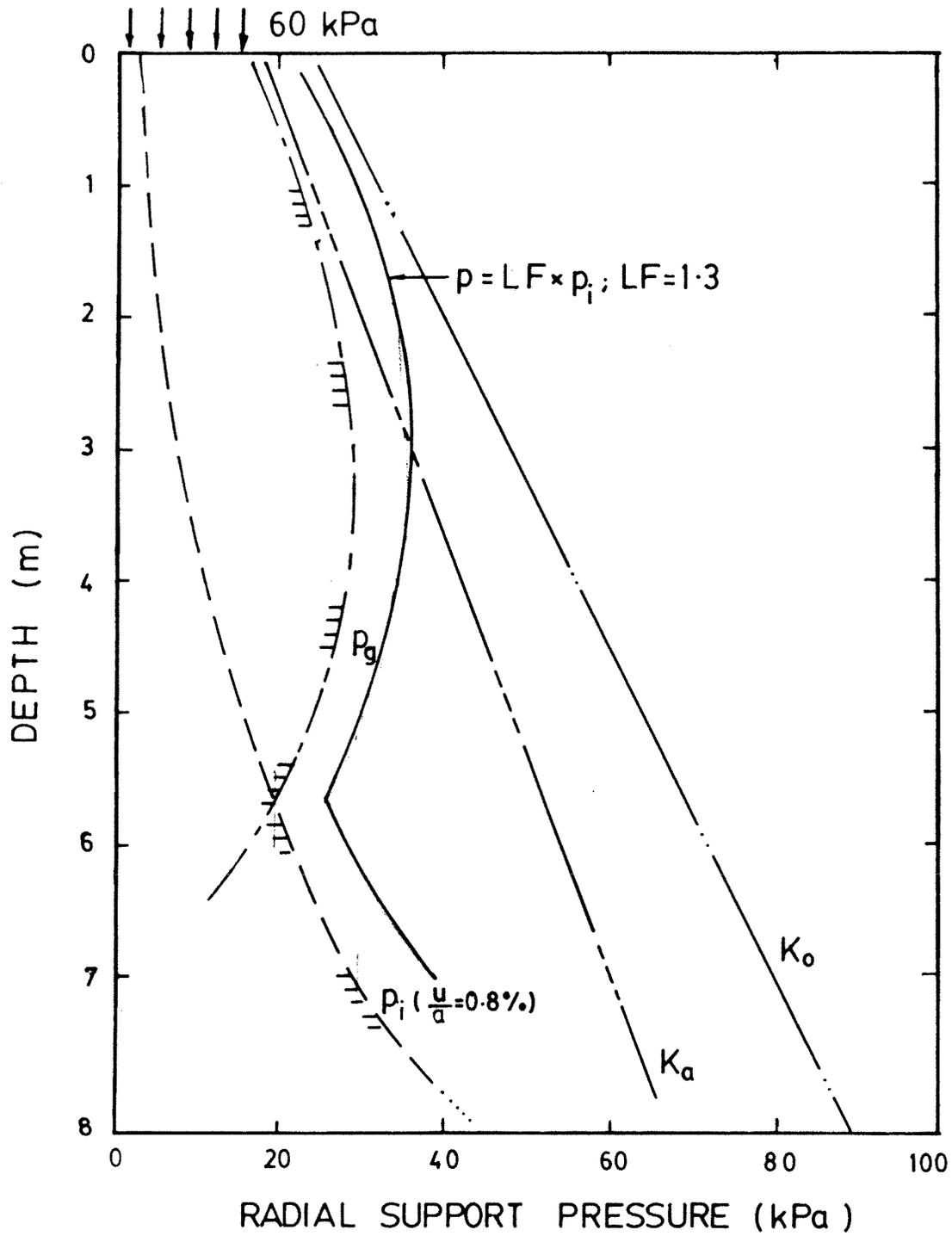| Stress Distribution around opening | Stress State at shaft wall |
|---|---|
| (1) | |
| (2) | |
| (3) | |

(b)
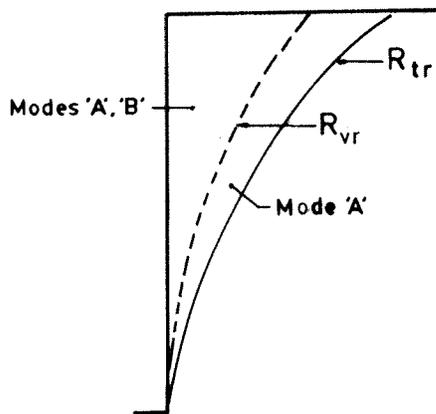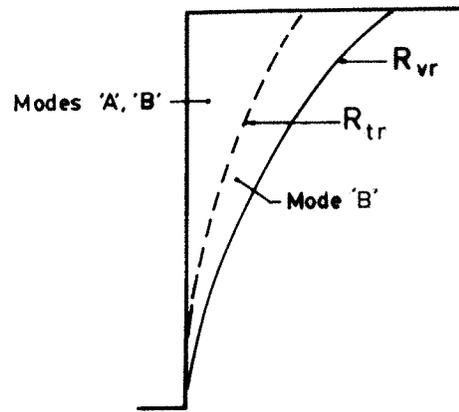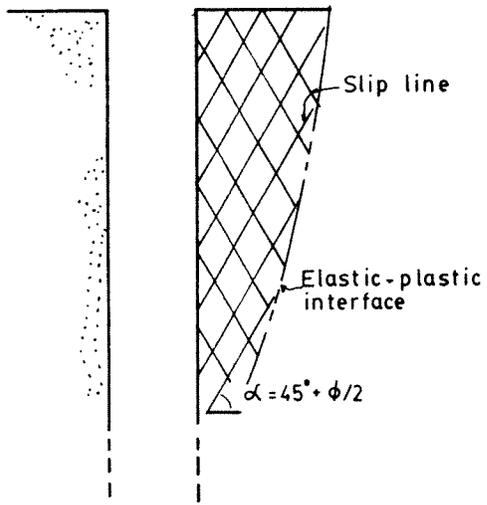
Wong and Kaiser (I+II) Fig. 6
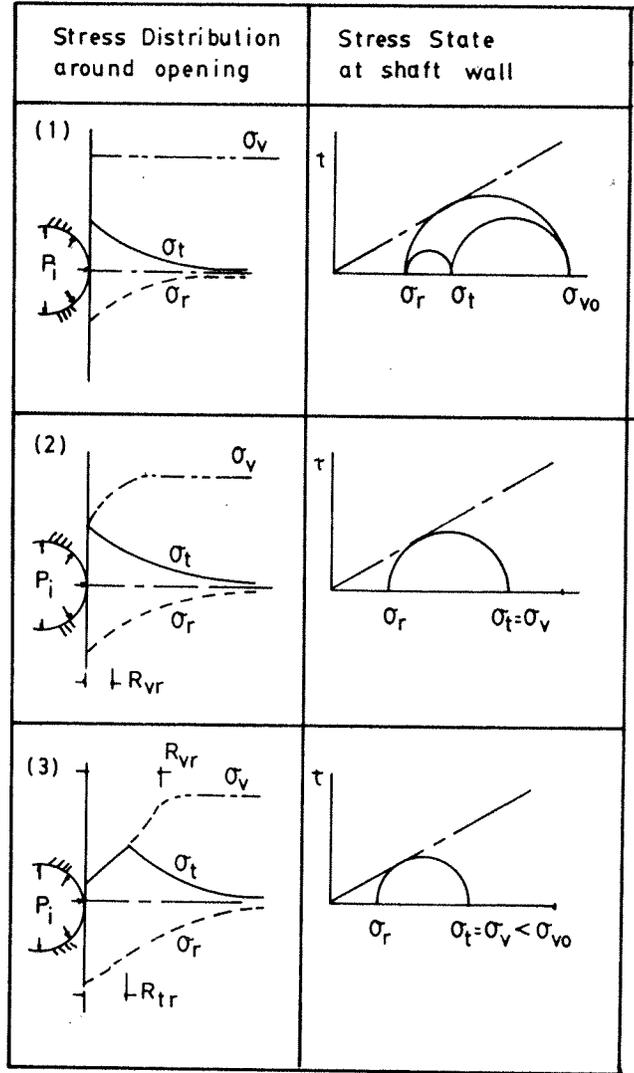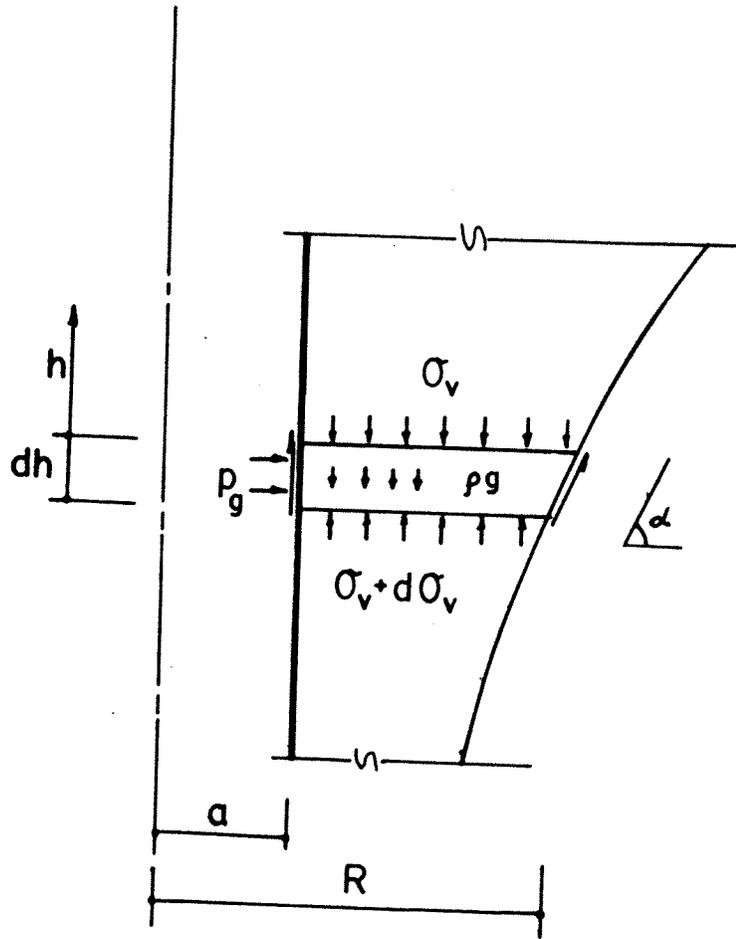
Wong and Kaiser (I+II) Fig. 7
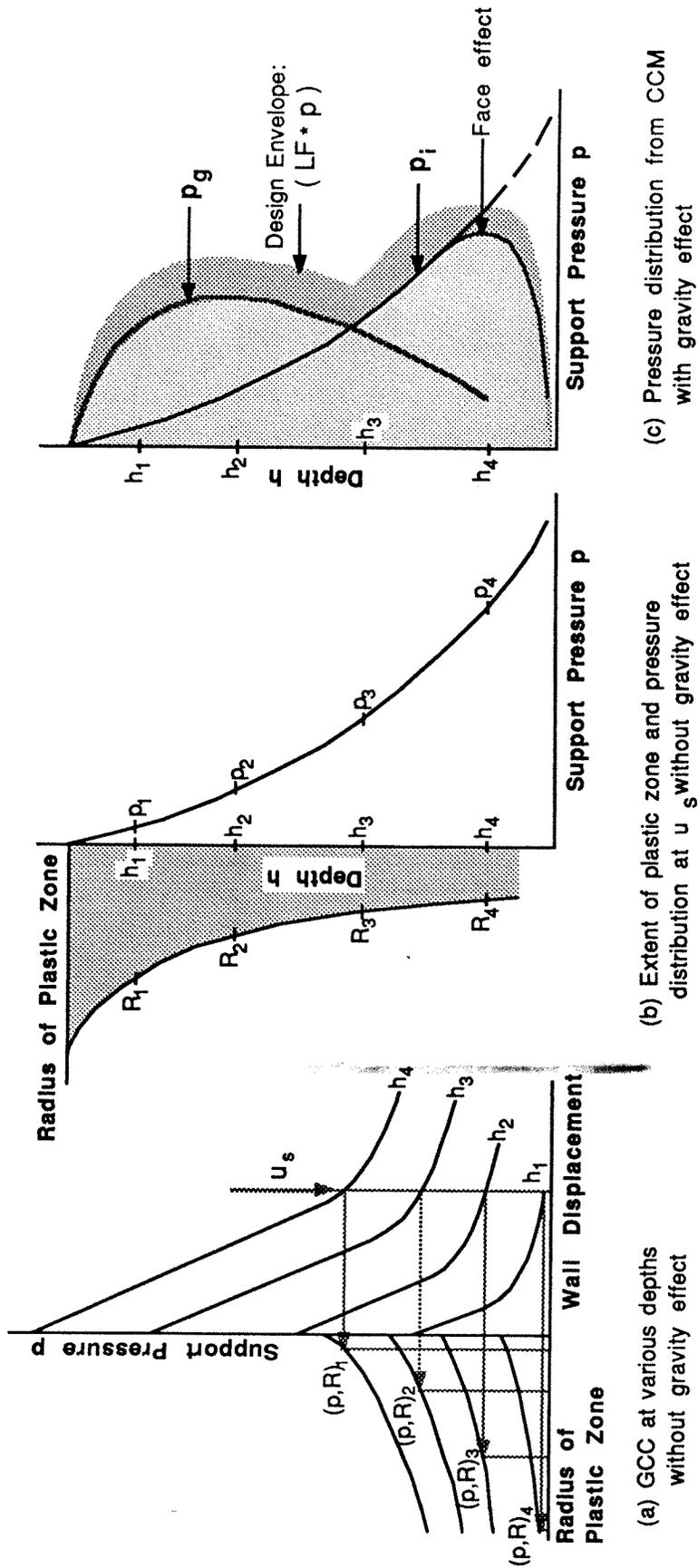
(a) GCC at various depths without gravity effect

(b) Extent of plastic zone and pressure distribution at $u_s$ without gravity effect

(c) Pressure distribution from CCM with gravity effect

Wong and Kaiser (I+II) Fig. 8

DISTANCE

DEPTH
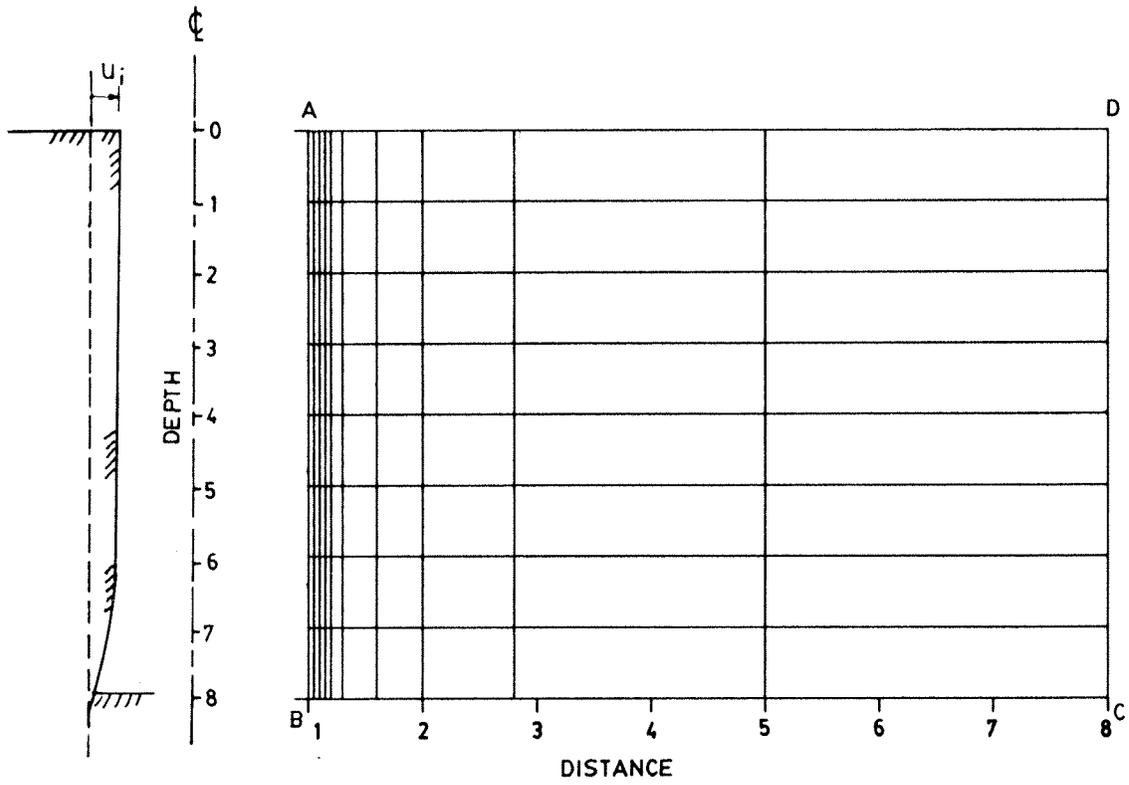
Wong and Kaiser (I+II) Fig. 9
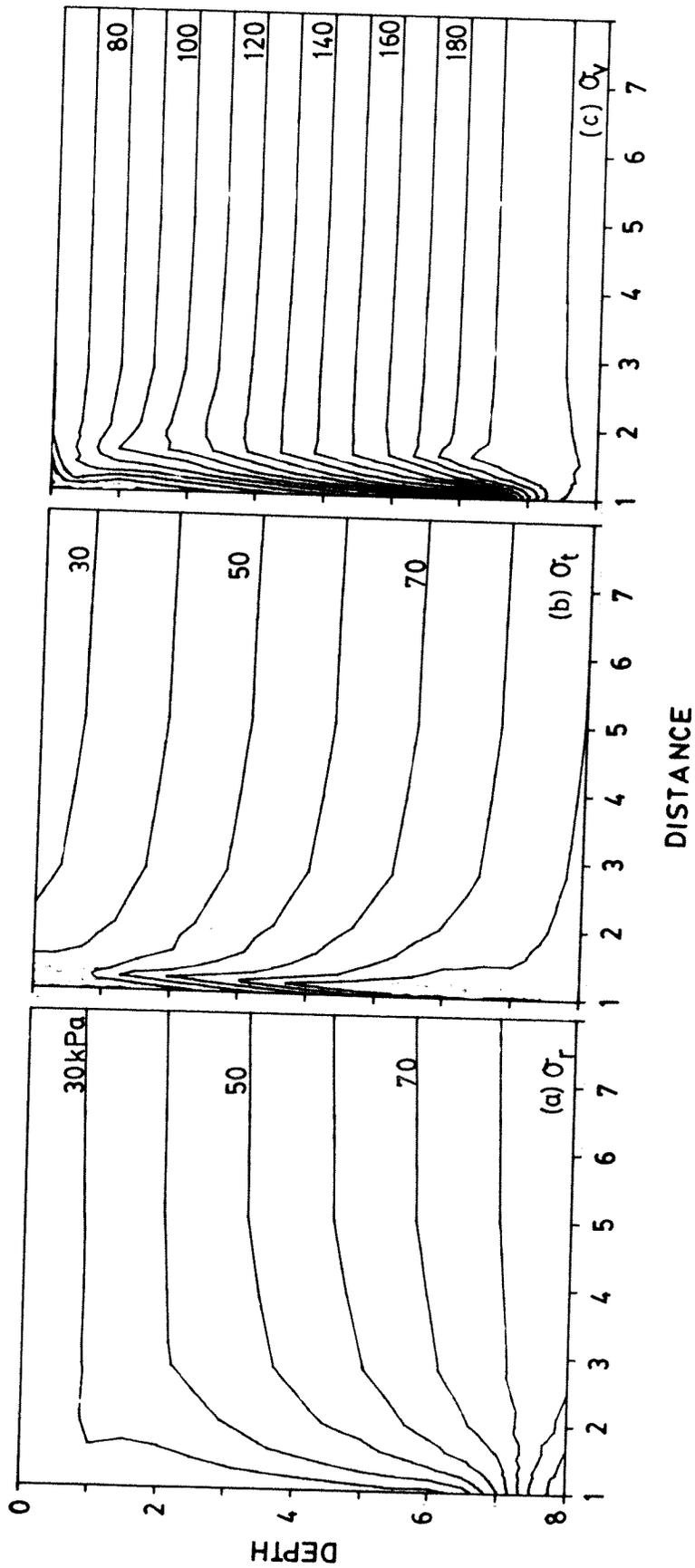
Wong and Kaiser (I+II) Fig. 10
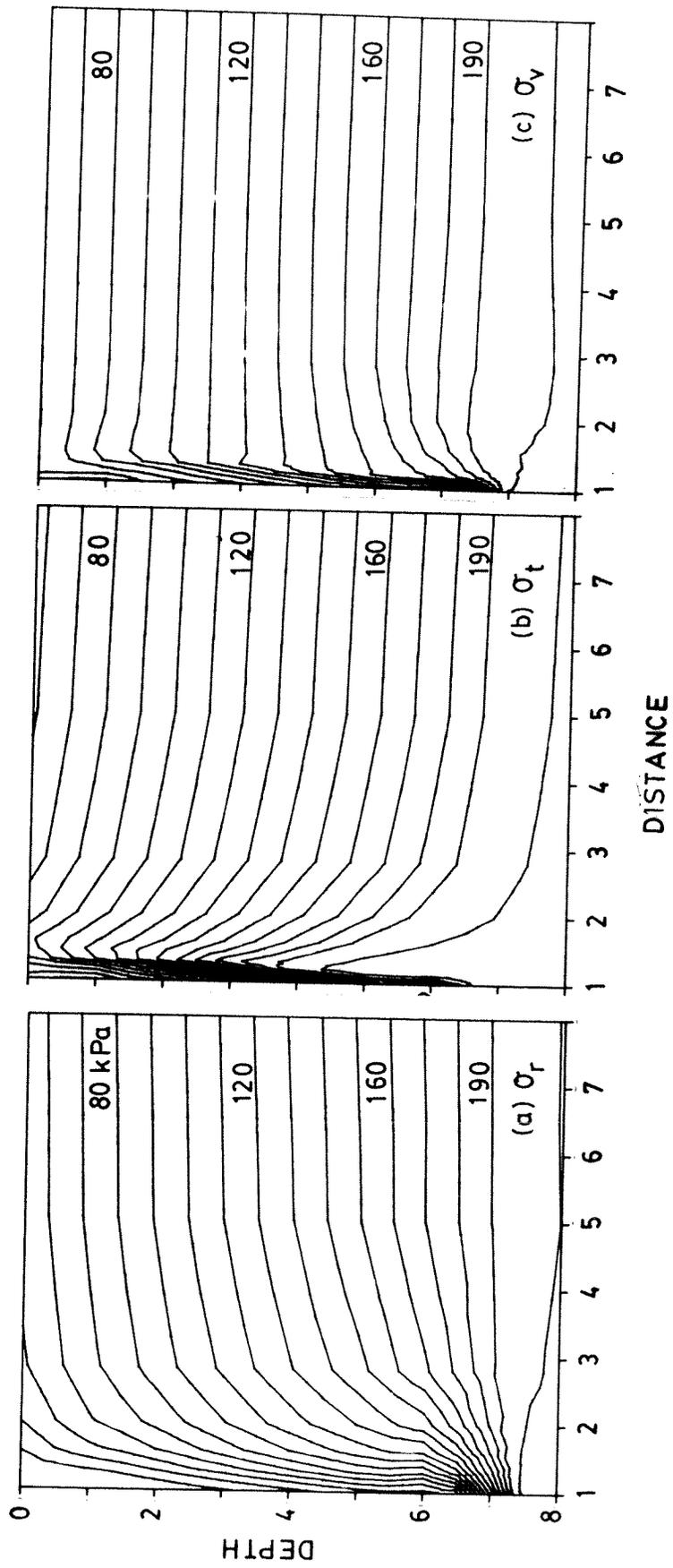
Wong and Kaiser (I+II) Fig. 11

Wong and Kaiser (I+II) Fig. 12

Cohesionless, Ko=0.98 (SM2)

FEM:
□ Radial Stress at u/a = 0.26%
○ Tangential Stress at u/a = 0.26%
△ Vertical Stress at u/a = 0.26%

+ Radial Stress at u/a = 0.5%
✕ Tangential Stress at u/a = 0.5%
◇ Vertical Stress at u/a = 0.5%

CCM:
Radial Stress at u/a = 0.26%
Tangential Stress at u/a = 0.26%

Radial Stress at u/a = 0.5%
Tangential Stress at u/a = 0.5%

STRESS (kPa)

DISTANCE FROM WALL (m)

Wong and Kaiser (I+II) Fig. 13

Wong and Kaiser (I+II) Fig. 16

Cohesionless, Ko=0.41

Cohesionless, Ko=0.98

Cohesive, Ko=0.98

Depth (m)

0.5

2.0

3.5

5.0

6.5

8.0

FEM:
□ □ u / a = 0.06 %
○ ○ u / a = 0.30 %
CCM:
—·— u / a = 0.06 %
— u / a = 0.30 %

FEM:
□ □ u / a = 0.26 %
○ ○ u / a = 0.50 %
CCM:
—·— u / a = 0.26 %
— u / a = 0.50 %

□ □ u / a = 0.20 %
○ ○ u / a = 0.56 %

1.0    1.6    2.2    2.8   1.0    1.6    2.2    2.8   1.0    1.6    2.2    2.8

Radial Distance from Shaft Wall (m)
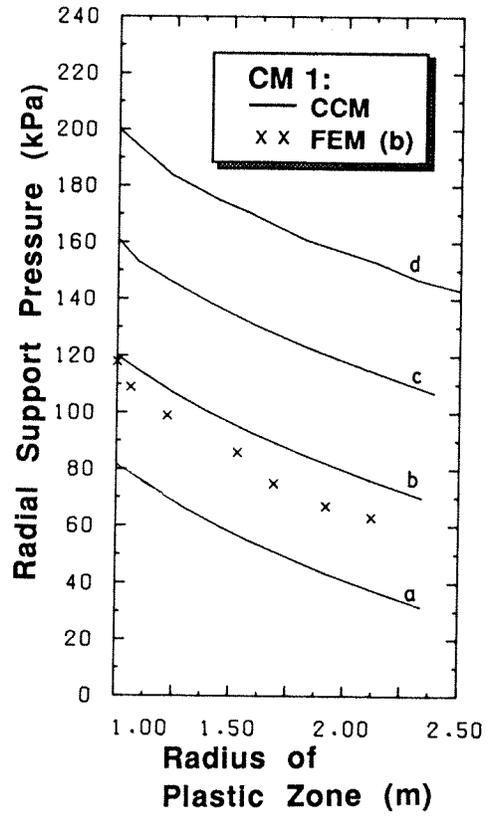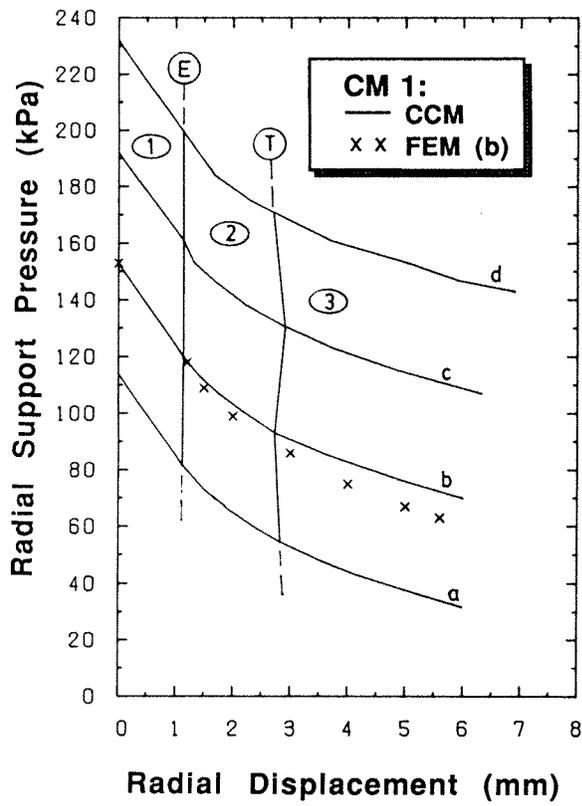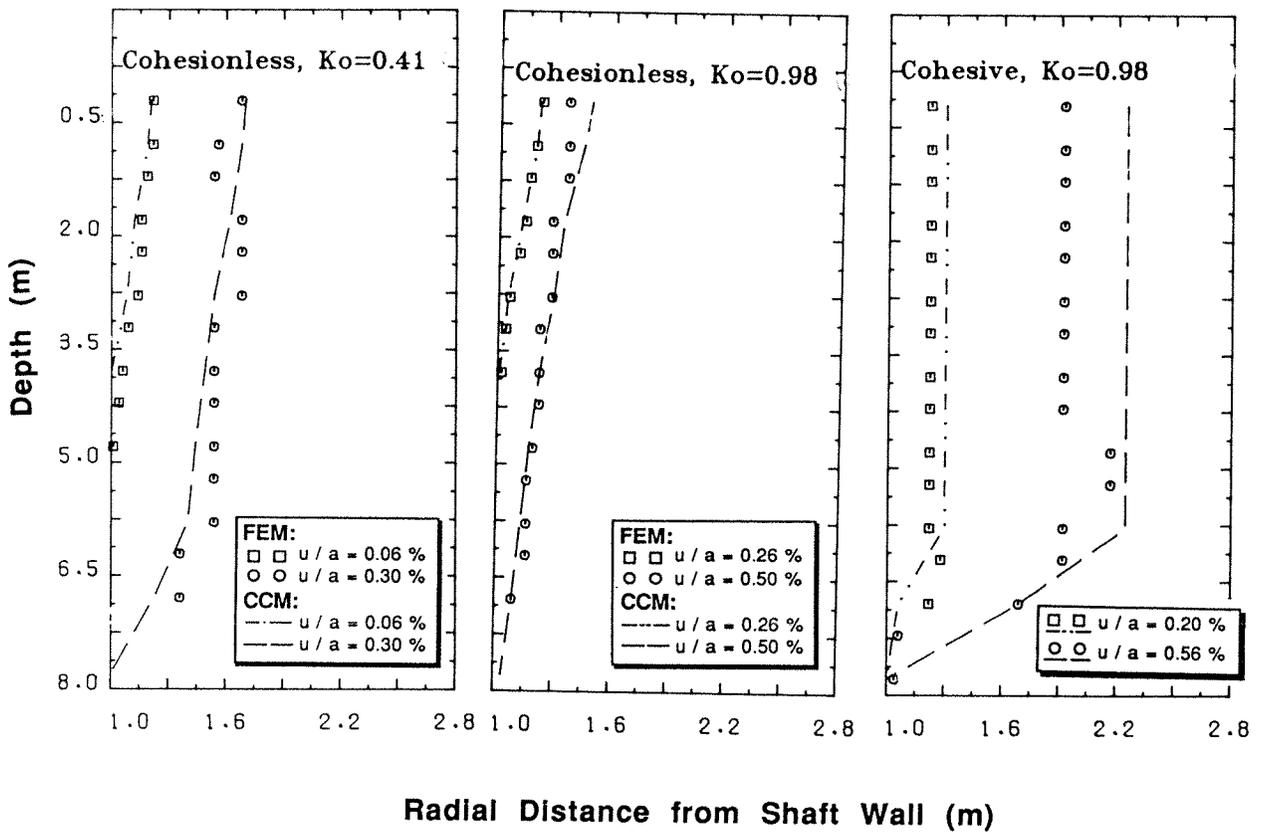
Wong and Kaiser (I+II) Fig. 17
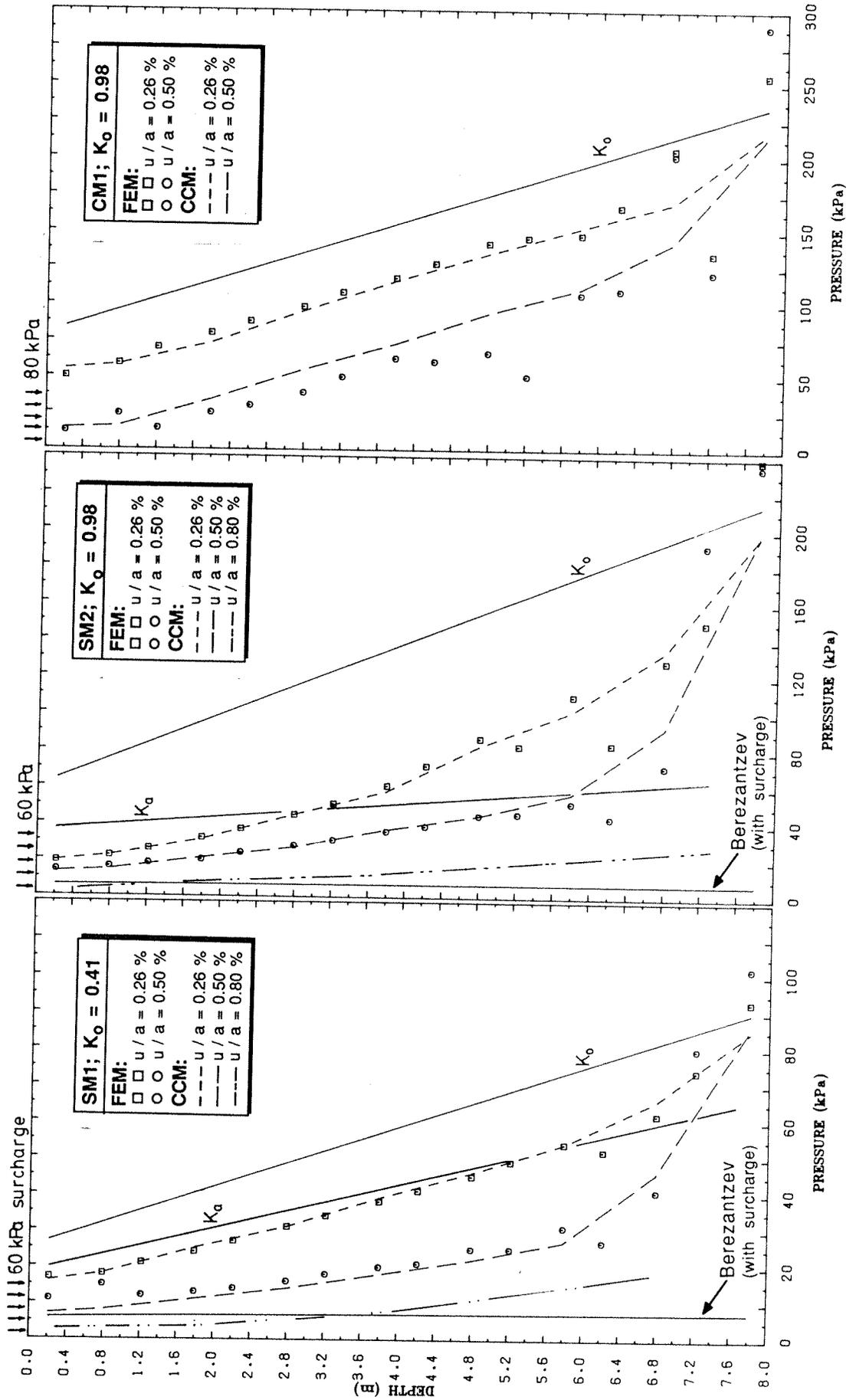
Wong and Kaiser (I+II) Fig. 18

(a) COHESIONLESS

Cohesionles Soil:
$a = 1m$
$\gamma = 20$ kN/m$^3$
$\phi = 30°$
$K_s = K_a = K_w = 0.33$

$K_a\gamma h$

$\beta = 80°$    $70°$    $60°$

Radial Support Pressure $p_g$ (kPa)

Depth (m)

Extent of Yield Zone
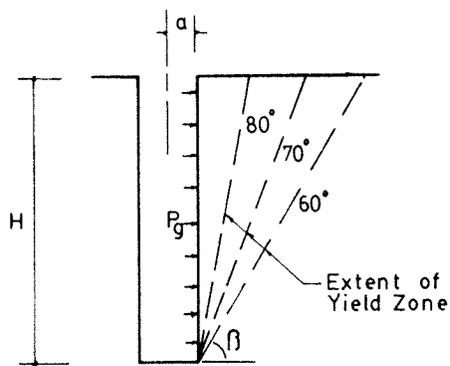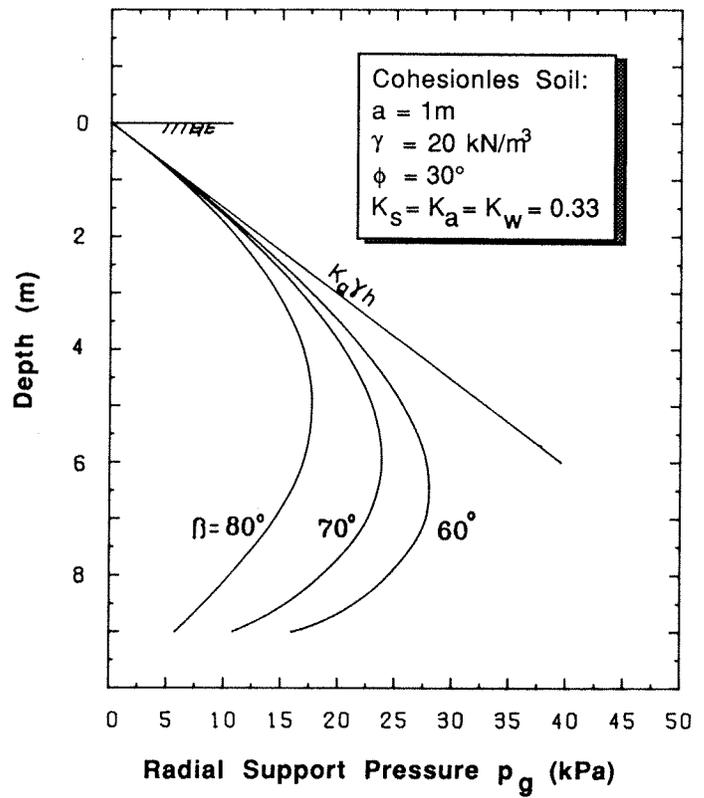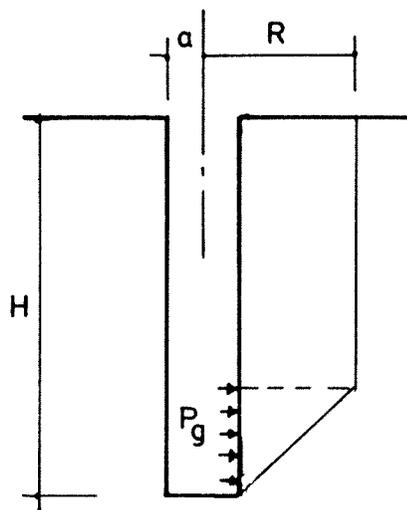
H = 10 m
a = 1 m
$C_u$ = 40 kPa

| R (m) | $P_g$ (kPa) |
|-------|-------------|
| 3     | 17          |
| 5     | 183         |

Wong and Kaiser (I+II) Fig. 20

Wong and Kaiser (I+II) Fig. 21

**Shaft Wall Displacement**

| COHESIONLESS | | COHESIVE | |
|---|---|---|---|
| MODE A $(K_{\bullet} > K_{cr})$ | MODE B $(K_{\bullet} < K_{cr})$ | MODE A $(K_{\bullet} > K_{cr})$ | MODE B $(K_{\bullet} < K_{cr})$ |
| E = Constant with depth | | E, $Q_u$= Constant with depth | |
| E = Increase with depth | | E, $Q_u$= Increase with depth | |
| | | E = Const. with depth ; $Q_u$=Increase with depth | |
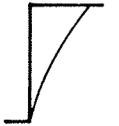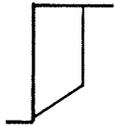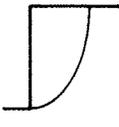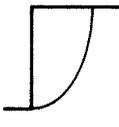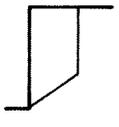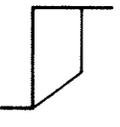
Wong and Kaiser (I+II) Fig. 23

Wong and Kaiser (I+II) Fig. C.1